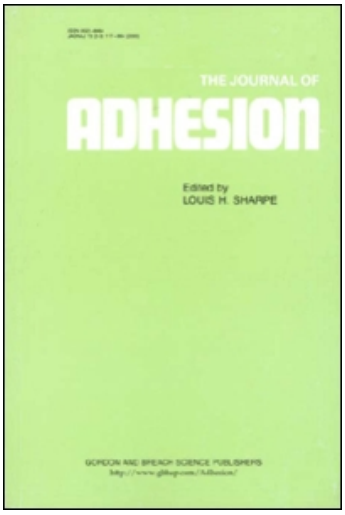

The Journal of Adhesion
Publication details, including instructions for authors and subscription information:
http://www.informaworld.com/smpp/title~content=t713453635

Electric-Field Induced Morphological Transitions in Elastic Contact Instability of Soft Solid Films

N. Arun[a]; J. Sarkar[b]; Ashutosh Sharma[b]; V. B. Shenoy[c]; K. S. Narayan[a]
[a] Jawaharlal Nehru Centre for Advanced Scientific Research, Bangalore, India [b] Department of Chemical Engineering, Indian Institute of Technology, Kanpur, India [c] Material Research Centre and Centre for Condensed Matter Theory, Indian Institute of Science, Bangalore, India

To cite this Article Arun, N. , Sarkar, J. , Sharma, Ashutosh , Shenoy, V. B. and Narayan, K. S.(2007) 'Electric-Field Induced Morphological Transitions in Elastic Contact Instability of Soft Solid Films', The Journal of Adhesion, 83: 6, 513 — 534
To link to this Article: DOI: 10.1080/00218460701453486
URL: http://dx.doi.org/10.1080/00218460701453486

The Journal of Adhesion, 83:513–534, 2007

ISSN: 0021-8464 print/1545-5823 online
DOI: 10.1080/00218460701453486

Taylor & Francis
Taylor & Francis Group

Electric-Field Induced Morphological Transitions in Elastic Contact Instability of Soft Solid Films

N. Arun
Jawaharlal Nehru Centre for Advanced Scientific Research, Bangalore, India

J. Sarkar
Ashutosh Sharma
Department of Chemical Engineering, Indian Institute of Technology, Kanpur, India

V. B. Shenoy
Material Research Centre and Centre for Condensed Matter Theory, Indian Institute of Science, Bangalore, India

K. S. Narayan
Jawaharlal Nehru Centre for Advanced Scientific Research, Bangalore, India

A soft elastic film, when placed in adhesive proximity with a contactor in a crack-like geometry, spontaneously undergoes a surface instability to form finger patterns with a characteristic wavelength of approximately 4h, where h is the film thickness. We study the morphological evolution and control of this elastic contact instability under the influence of an external electric field. The distinct electric field induced morphological changes, leading to the formation of two-dimensional hexagonally arranged pillars, large-amplitude fingers, and straightening of contact edge, which are studied comprehensively. The conditions for the evolution of morphologically distinct patterns are governed by the film parameters, such as its shear modulus and thickness. A theoretical model and its stability analysis provide an approximate estimate of the critical voltage required for the onset of changes and its scaling with the film parameters (thickness and shear modulus). Further, three-dimensional simulations based on energy minimization are presented to provide important clues regarding the physics of pattern evolution on soft elastic interfaces.

Received 20 November 2006; in final form 7 March 2007.
Address correspondence to K. S. Narayan, Jawaharlal Nehru Centre for Advanced Scientific Research, Jakkur, Bangalore 560064, India. E-mail: narayan@jncasr.ac.in

Keywords: Electric field; Meniscus instability; PDMS; van der Waals forces

1. INTRODUCTION

Interfaces, especially involving thin soft films, are important in many technological applications and offer a plethora of fundamental scientific problems. Spontaneous formation of patterns during adhesion and debonding and the accompanying deformation at soft interfaces is an area of active investigation because of its importance in industries ranging from interface engineering to biology and medicine [1–7]. A fascinating aspect of interface physics is the existence of many competing energies, which can give rise to a myriad of morphological patterns and structures. Understanding the precise origin and form of these patterns can also provide important clues to *control* these morphological instabilities with potential technological applications at the micro- and nanoscales.

Both liquid and solid films show morphological instabilities under the influence of external fields such as the long-range van der Waals and electric fields. In liquid films, excess intermolecular interactions compete with the surface energy, resulting in a long-wave surface instability and self-assembled morphological patterns [8–10]. An important aspect of the morphological instabilities in liquid films is that the wavelength of the patterns is a very strong function of the competing energies, the external field, and the surface tension that together modulate the instability. There have been several attempts to *control* these instabilities for engineering of mesoscale patterns. For example, dewetting instability of a liquid film on a physicochemically patterned substrate can be used to generate patterns of various shapes and morphologies [11]. Another promising route may be found in the work of Schaffer and coworkers [12–14], who used an external electric field to control the surface instability and to generate desired mesopatterns. The length scale of these patterns, and the final spacing obtained, is a strong and nonlinear function of the film thickness, strength of the electric field, and the film's surface tension.

Solid films are also susceptible to a variety of field-induced surface instabilities. In "hard" films, surface patterns appear because of the competition between elastic strain energy and surface energy [15–19], causing a chemical potential gradient that drives mass diffusion, resulting in an irreversible pattern in the film. Material nonlinearities (plasticity, for example) can also give rise to patterns in these films [20]. Recently, a new type of instability was discovered in *soft elastic* thin films

[21–24]. When a curved contactor is placed near a soft film, producing a crack-like geometry between the surface of the film and that of the contactor, the contact meniscus assumes a pattern with periodically spaced fingers [21]. Interestingly, the spacing between these fingers was found to be independent of all the controllable experimental parameters (shear modulus of the film, the contactor–film interaction, etc.) but showed a linear dependence on the film thickness (about four times the film thickness). In different experiments [22,24] with a different geometry consisting of a nearly flat contactor approaching the film, it was found that the film surface undergoes an instability that has a two-dimensional character. Further, the wavelength of these patterns was also found to be independent of all the parameters other than the film thickness—the wavelength of these patterns in this case was also found to be again about three to four times the film thickness. The physics of these patterns was traced to the competition between the attractive van der Waals type adhesive interactions between the contactor and the film surface, which acts to drive the instability, while the stored elastic energy acts as the stabilizing factor [25]. Once the adhesive interaction exceeds a critical value (determined by the distance of the contactor from the film surface, usually 20–100 nm), the film surface assumes a patterned morphology with a wavelength of about three times the film thickness. Some aspects of this instability have been studied recently [26–33]. In particular, the instability is shown to have a profound effect on the adhesion of soft films [32] and, further, has the potential of developing into a soft lithography technique for patterning of soft films [31].

However, the contact instability of elastic films is difficult to control. This is because the adhesive forces engendered by the intermolecular interactions are very short ranged and hard to modulate. The contact patterns can therefore be strongly influenced by such difficult-to-control factors as the film surface roughness and defects, even of very small dimensions. Therefore, it is desirable to use the physics of the contact instability described previously to control the film morphology but with a method that allows for a far greater flexibility in control and modulation.

In this article, we show that an externally applied electric field can strongly modulate the surface instability in the film. The application of an electric field on pre-existing finger patterns (such as that in Ref. [21]) is used to control their dimensionality and morphology. We elaborate the results of our recent observations [34], where we demonstrate experiments that show three distinct morphological modifications, which we call “edge straightening,” “finger elongation,” and “pillar formation,” along with theoretical models that explain these effects. We present results consistent with the earlier speculation

explaining the origin of these field-induced features. Our work provides a new method for the *control* of the surface instability (and resulting morphology) in the soft elastic films and has the potential of providing a nonlithographic route to patterning. Controlling the surface morphology and adhesion of a soft interface by electric fields may also have applications in structural modifications in microfluidics [35], smart adhesives, and soft lithography [36,37].

2. EXPERIMENTAL

A transparent conducting indium tin oxide (ITO) (Praezisions Glas & Optik GmbH, Iserholn, Germany)–coated glass was used as the substrate on which the soft cross-linked poly-dimethyl siloxane (PDMS) films were coated. The substrate was cleaned using ultrasonication in deionized water, acetone, and isopropanol and was then flow dried under an N_2 atmosphere. The polymer, PDMS (Sylgard-184, Dow Corning Chemicals, Midland, MI, USA), was then spin coated on this substrate. The thickness of the films varied from 10 μm to 100 μm by varying the spin coater speed (500 to 4500 rpm). The sylgard-184 cross-linker concentration (2% to 10%) was varied to obtain different shear modulus for the films ($1\,\text{MPa} < \mu < 8\,\text{MPa}$). These films were then annealed at 60°C for 4 h to obtain the uniform, soft, elastic films. The thickness of the films was determined by standard analysis from the interference patterns in the transmission spectroscopy measurements [38].

The schematic of the experimental setup is shown in Figure 1. A 100-μm spacer was placed on one end of the film. A flexible contactor (cover glass 2.2 cm × 2.2 cm, thickness ∼225 μm) (Corning Incorporated, Lowell, MA, USA) was placed on the elastic film such that one end of the contactor was in contact with the film and the other end was supported on top of the 100-μm spacer. The flexible contactor had a semitransparent coating of chromium-gold (Cr thickness ∼20 nm and Au thickness ∼50 nm) on its top surface. A high voltage breakdown tester (Keithley Instruments, Cleveland, OH, USA) was used to apply the voltage between the chromium-gold electrode and the ITO electrode. The patterns were observed under a microscope, and the images were captured using a charge-coupled device (CCD) camera. To avoid arcing and shorting between the electrodes, the gold-coated side of the contactor was kept on top, and the other noncoated side was in contact with the film. Even though this arrangement required application of high voltages (∼1000 V) for the initiation of the instability, it avoided the problem of shorting and polymer breakdown that we consistently saw in the arrangement when the metal was in direct contact with the film. However, it may be noted that the actual voltage the film was subjected

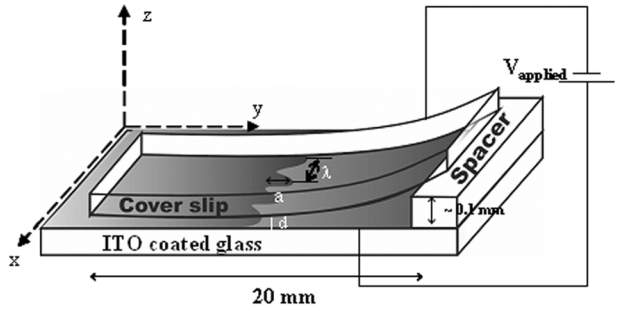

(a)

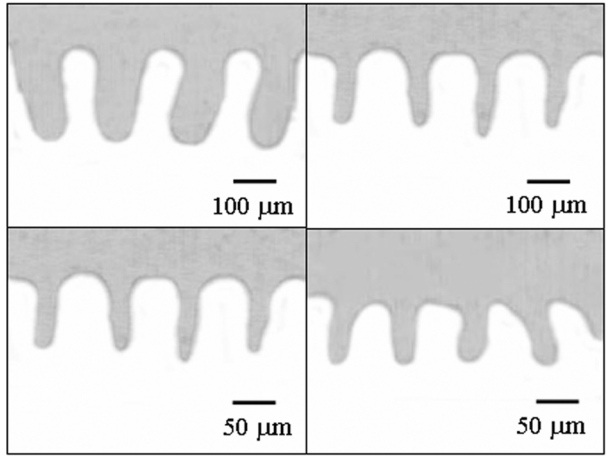

(b)

FIGURE 1 (a) Schematic of the experiment and the finger pattern of wavelength λ. The dark part of the film depicts the contact region. (b) The finger patterns observed prior to the application of the external electric fields for different thickness and shear modulus: clockwise $h = 37.2\,\mu m$ and $\mu = 3.9\,MPa$, $h = 43.3\,\mu m$ and $\mu = 6.9\,MPa$, $h = 29.9\,\mu m$ and $\mu = 2.2\,MPa$, and $h = 24.1\,\mu m$ and $\mu = 3.0\,MPa$, respectively.

to in this arrangement is far less than the nominal applied voltage because of the voltage drop across the glass cover.

3. RESULTS

A zone of complete adhesive contact between the film and the contactor terminated in a periodic finger pattern near the crack tip, where zones of periodic adhesive contacts formed. An air gap (d) was present

ahead of the finger pattern, which increased gradually along the y-direction away from the patterns. Well-defined finger patterns (Figure 1b) with wavelength $\lambda \sim 4h$, which formed because of the adhesive van der Waals interactions alone [21], were ensured before the application of the voltage.

The external voltage induced changes to the existing fingering pattern. The observed effect of electric field was broadly classified into three different regimes. The morphological changes witnessed depended mainly on the shear modulus and the film thickness. These regimes were classified as (a) "pillar formation" regime, (b) "finger elongation" regime, and (c) "edge straightening" regime. These morphological transitions can be understood in terms of the stiffness parameter of the films, (μ/h), which is the ratio of the shear modulus and the film thickness. Edge straightening and finger elongation were observed for high and intermediate stiffness (μ/h) films, whereas for low (μ/h) films, pillar formation was observed. The patterns in edge straightening and pillar formation correspond to a change in the dimensionality of the pattern [34].

3.1. Pillar Formation

In case of films with low shear modulus ($1\,\text{MPa} < \mu < 4\,\text{MPa}$), additional morphological features arise beyond a critical value of the electric field. Beyond a critical voltage (ϕ_c), a row of pillars of nearly circular cross-sections emerged ahead of the fingers. These pillars rise up to adhere to the contactor and emerge in the region ahead of the finger patterns as seen in Figure 2a. Interestingly, the emergence of pillars does not change the arrangement and morphology of the pre-existing finger pattern. Further increase in the voltage caused additional rows of pillars to emerge at the farther side of the gap in tandem with the increased diameter of the existing pillars (Figure 2a). These pillars formed a two-dimensional (2-D) hexagonal-type arrangement with the spacing along both the x- and y-directions of these pillars, similar to that of the adjacent finger pattern. As the distance from the finger patterns increased (along the y-direction), the diameters of the pillars reduced as shown in the inset in Figure 2a. This variation of the diameter of the pillars is due to the inhomogeneity in the electric field due to the inclined plane geometry. The application of the electric field increased the contact area between the film and the top contactor. As there was no appreciable change in the finger pattern, the contact area increase was achieved by newly formed pillar-like structures arising ahead of the finger pattern. Upon switching off the electric field, the pillars do not disappear or even relax in their morphology

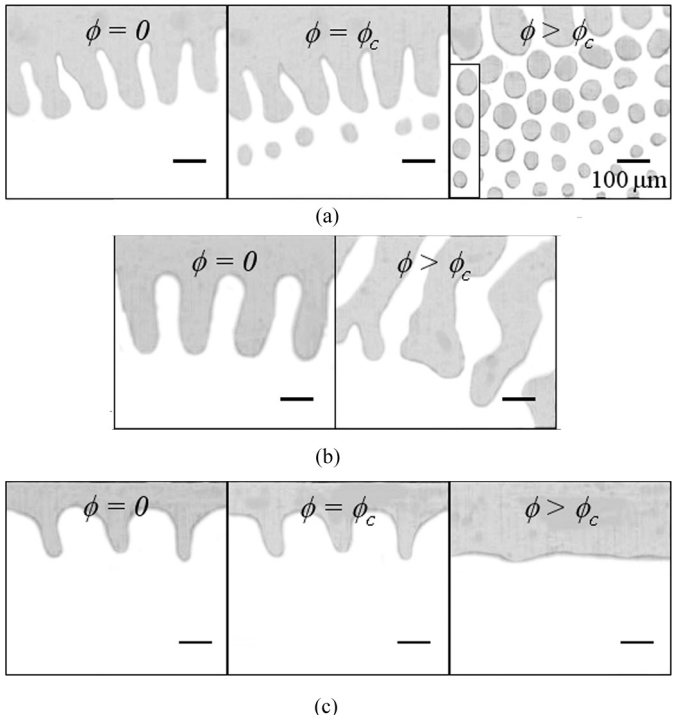

FIGURE 2 (a) Evolution of the pillars upon application of voltage for film parameters, $h = 43.17\,\mu m$ and $\mu = 2.17\,MPa$. Inset shows the decrease in diameter of the pillars as a function of distance away from the line of contact. (b) The elongation of the finger pattern for intermediate stiffness parameter films ($h = 37.2\,\mu m$ and $\mu = 3.9\,MPa$). (c) The edge straightening of the finger patterns for film parameters, $h = 76.8\,\mu m$ and $\mu = 6.9\,MPa$.

over an observation period of 24 h. This indicates that even though an external field exceeding a critical strength is necessary for the formation of pillars, the pillars, once formed, represent a locally stable or metastable configuration sustained solely by the contact adhesive forces. The pillar patterns relax back to the original configuration of the uniform film only after complete removal of the top contactor.

3.2. Labyrinth Formation

For films with intermediate shear modulus ($4\,MPa < \mu < 6\,MPa$), the electric field effects are qualitatively different. Beyond the critical voltage (ϕ_c), there was an abrupt increase in the amplitude of the

finger pattern by about an order of magnitude (Figure 2b). The wavelength of the fingers remained unaltered for small increases in the amplitude. Figure 3A shows the change in the amplitude ($\Delta a/a_{ini}$) with the applied voltage ϕ. Beyond the critical voltage ϕ_c, the fingers continued to elongate and eventually underwent multiple tip splitting, leading to the formation of patterns with a network of interpenetrating fingers as shown in Figure 2b. The electric field in this case increased the adhesive contact area by increasing the amplitude (length) of the patterns and later by the formation of split fingers. The change in the distance of the contact line and the basic finger morphology was minimal. Again, it was observed that the labyrinth formation was irreversible; *i.e.*, upon switching off the voltage, the patterns remain trapped in the local metastable state and do not relax back to the original configuration of short amplitude fingers. The film regains its original flat configuration only upon removal of the contactor. It was noticed that the finger elongation was sensitive to the degree of bending of the contactor, with the occurrence of prominent finger elongation for flexible constraints. Another set of observations in this regard was that the precursor finger pattern upon contact is not necessary to observe the labyrinth pattern. A nonuniform electric field (beyond the critical electrical field at x = 0) formed by an inclined top flexible constraint that is not in contact with the elastic film also leads to a labyrinth

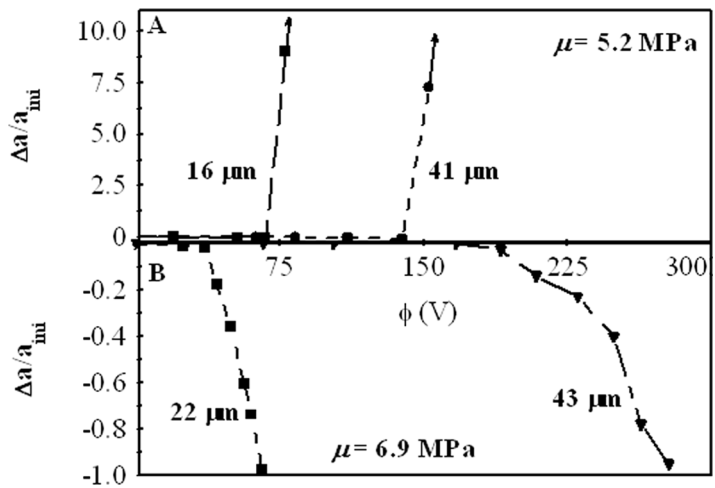

FIGURE 3 Change in amplitude ($\Delta a/a_{ini}$) upon applying the voltage ϕ. (A) $\mu = 5.2$ MPa for various film thickness ($h = 16\,\mu$m and $41\,\mu$m). (B) $\mu = 6.9$ MPa MPa for various film thickness ($h = 12\,\mu$m and $43\,\mu$m).

formation. If the flexible constraint (cover glass slide) is replaced by a stiff glass slide, the labyrinth formation is suppressed.

3.3. Edge Straightening

In contrast to the previous two cases, the response of high shear modulus films ($\mu > 6\,\text{MPa}$) to an external electric field was edge straightening. Beyond ϕ_c, the amplitude of the finger patterns *reduced* without any appreciable change in its characteristic wavelength or periodicity. It was observed that the straightening of the finger pattern occurred asymmetrically, with the amplitude of the finger decreasing with respect to the stationary tip as shown in Figure 2c. Further, the finger patterns straightened eventually to form a linear edge ($a \to 0$ or $(\Delta a/a_{ini}) \to -1$) at a much higher voltage ϕ. The variation of amplitude with the applied voltage is shown in Figure 3B. The increase in the contact area between the film and the top glass contactor was accomplished by an outward displacement of the crack tip or contact line, with a simultaneous decrease in the amplitude of the fingers. The adhesive contact thus enlarged but became more uniform. Eventually, the fingers disappeared, leading to edge straightening. Further increase in the voltage resulted in a gradual displacement of this linear edge toward regions of lower electrostatic energy and, thus, a further increase in the contact area. Thus, the contact line becomes less undulating, and the distance to the contact line increased, indicating a more intimate contact and larger area of contact between the film and the top glass substrate, as depicted. ϕ_c does not depend significantly on the ramping rate or on the polarity of the voltage but depends mainly on the electrostatic energy as explained in the discussion section. Unlike the other two cases discussed earlier, the edge straightening behavior is observed to be reversible: the initial small-amplitude fingers reappear upon switching off the voltage. However, the process of recovery was slow (the recovery time was $\sim 30\,\text{min}$). The time taken for the reappearance

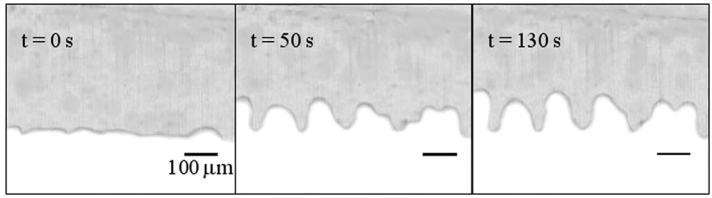

FIGURE 4 Hysteresis effect: The slow relaxation of the intimate contact after switching off the voltage ϕ at different times for film with $h = 43.3\,\mu\text{m}$ and $\mu = 6.9\,\text{MPa}$.

of the finger pattern depended on the material properties such as the shear modulus and the thickness. This dynamic hysteresis effect can be observed in Figure 4, where the relaxation back to the original finger pattern upon switching off the field took a much longer time than the edge-straightening behavior upon switching on the electric field. The latter was almost instantaneous.

4. DISCUSSION

Theoretical arguments that uncover the physics of these observations are discussed. There are two aspects to the theoretical arguments; first is the formulation of an appropriate energy functional that captures the essential physics, and second is the analytical calculation and numerical results obtained from the study of the energy functional.

In the present experiments, we start with a pre-existing finger pattern formed by adhesive contact without an electric field. These patterns, as noted previously [25], are a result of the competition between the attractive van der Waals forces between the contactor and the film surface and the restraining elastic energy of the film. Our goal is to understand how the electric field produces *changes* in the morphological patterns. To this end, we develop an energy functional keeping only the electric field effects, and as a first approximation, ignore the contribution of van der Waals force as the changes are observed even at large d (>100 nm). It was observed that the electric-field-induced phenomenon does not vary significantly for a wide range of differently treated top contactor surfaces. There were marginal changes in finger-pattern amplitudes but the responses with respect to the electric field were equivalent. We now show that the electric field produced in the gap (Figure 5) acts to *promote morphological changes*; in particular, the electric field acts as a *destabilizing force*. The stabilizing influence in the system, as in the previous work, arises from the elastic energy of the nearly incompressible films. To obtain an energy functional that contains this physics, we note that the *electrostatic energy* of the system shown schematically (Figure 5) is

$$\Pi_{ES}(Q,\phi) = \frac{1}{2}CQ^2 - \phi Q, \tag{1}$$

where C is the *effective capacitance* of the part of the system of interest, ϕ is the *effective voltage drop* across the air gap of thickness d and the PDMS film (Figure 5), and Q is the as-yet-undetermined charge stored. For a given voltage ϕ, the charge that builds up in the system minimizes the electrostatic potential energy [39] Π_{ES} and equals

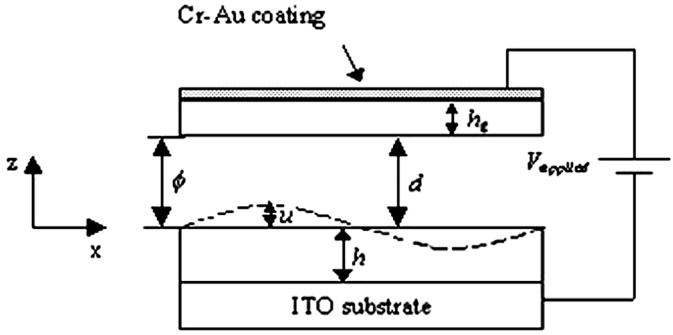

FIGURE 5 Schematic of the model used to explain the effect of electric fields. The effective voltage (ϕ) experienced by the film surface is $\sim V_{applied}/[1+\{(\varepsilon_g/\varepsilon_p)(h/h_g)\}]$, where $V_{applied}$ is applied voltage, ε_g and ε_p and h_g and h are relative dielectric constants and thickness of glass and PDMS, respectively.

$$Q = \frac{\phi}{c}.$$

The electrostatic energy in terms of the potential ϕ can be expressed as

$$\Pi_{ES} = -\frac{1}{2}C\phi^2. \tag{2}$$

The effective capacitance C can be obtained to a simple approximation by the following argument. Consider a plane capacitor with a total gap of $(h+d)$ filled partially with a dielectric material (dielectric constant ε_p) to a thickness h and with the air gap d. The effective capacitance per unit area C of the this capacitor is given by

$$C = \frac{\varepsilon_0\varepsilon_p}{\varepsilon_p d + h},$$

where ε_0 is the permittivity of a vacuum. Surface deformation increases the film thickness from h to $(h+u)$, where u is the normal displacement of the film surface along the z direction (Figure 5). The local air gap thus changes to $(d-u)$, and the resulting capacitance now is

$$C(u) = \frac{\varepsilon_0\varepsilon_p}{\varepsilon_p d + h - (\varepsilon_p - 1)u}.$$

It is evident that if $\varepsilon_p > 1$ (a condition that is obviously satisfied in our PDMS films, $\varepsilon_p = 3$), the *capacitance increases if the effective film thickness increases by a displacement of the film surface*. Thus we

see that, for a given potential ϕ, the electrostatic energy provides an attractive force between the contactor surface and the film surface.

In reality, the surface deformation u will not be a constant, especially because the film is nearly incompressible. In such a condition, an approximate expression for the effective capacitance can be obtained by using the expression for the capacitance per unit area $C(u)$ as

$$C = \int_A dx\ dy C(u(x,y)) = \int_A dx\ dy \frac{\varepsilon_0 \varepsilon_p}{\varepsilon_p d + h - (\varepsilon_p - 1)u(x,y)}, \qquad (3)$$

and, consequently, the electrostatic energy for the potential ϕ is now obtained as a functional of $u(x,y)$ as

$$\Pi_{ES}[u] = -\frac{1}{2}\int_A dx\ dy \frac{\varepsilon_p \varepsilon_0 \phi^2}{\varepsilon_p d + h - (\varepsilon_p - 1)u(x,y)}, \qquad (4)$$

which depends on ϕ^2 (not on the sign of ϕ), and A is the area of the film surface. As noted previously, there are two important approximations in writing Eq. (4). The first is that u varies slowly compared with the thickness of the film, and therefore, the approximation using Eq. (3) is not unreasonable. Second, the electrostatic potential distribution is consistently determined by the deformation of the film surface—we neglect this higher order effect. This could possibly be an oversimplification when studying the full nonlinear *evolution* of the film morphology but is not a serious limitation in the predictions of the critical voltage (to be explained later) for the onset of instability. This is because the deformations in the film before the onset of the electric-field-induced instabilities are small, with the consequence that the changes in electrostatic potential can be neglected.

The second important energy in the system is the elastic energy due to the deformation of the film induced by the electric fields. The elastic potential energy is written as

$$\Pi_{EL}[u] = \int_V dV W(\boldsymbol{E}), \qquad (5)$$

where $W(\boldsymbol{E})$ is the strain energy density, $\boldsymbol{E}$ is the strain tensor (gradient of displacements), and V is the volume of the film. The strain energy density depends on the shear modulus μ of the film; $W(\boldsymbol{E}) = 1/2(\mu\varepsilon) : \boldsymbol{E}$. The elastic energy *increases* if there is a deformation of the film and hence acts as a stabilizing factor in this system.

The total potential energy (for a given voltage ϕ) is a functional of the displacement field and is

$$\Pi[u] = \Pi_{EL}[u] + \Pi_{ES}[u] = \int_V dV W(E) - \frac{1}{2}\int_A dx\, dy \frac{\varepsilon_0 \varepsilon_p \phi^2}{\varepsilon_p d + h - (\varepsilon_p - 1)u(x,y)}. \tag{6}$$

We now use this energy functional to determine the critical voltage required to induce morphological changes.

As noted previously, the finger pattern induced by the van der Waals forces is ensured before the application of the potential, which implies that the surface deformation u is not only a function of x but also of the perpendicular direction y (Figure 1). To obtain an analytical expression for the critical voltage, we assume that the variation of deformation along the x-direction is much larger than in the y-direction and, hence, the variation along the y-direction is neglected. Within this framework, we now perform a linear stability analysis of Eq. (6). To this end, for a given gap thickness d and voltage ϕ, we note that the homogeneous state of the film comprises $u = 0$ (this is now the additional displacement to what is already present because of the preexisting finger pattern), with an additional uniform pressure field p_0 in the film, given

$$P_0 = \frac{(\varepsilon_p - 1)\varepsilon_0 \varepsilon_p \phi^2}{(\varepsilon_p d + h)^2}. \tag{7}$$

The pressure p_0 in Eq. (7) is obtained by calculating the force per unit area of the film surface exerted by the electric field. For a given d, if ϕ is large enough, this homogeneous state may be unstable to pattern formation. To investigate this, we assume that the film surface undergoes a perturbing deformation of the form

$$u(x) = \alpha_k \cos kx, \tag{8}$$

where k is the wavevector of the perturbation and α_k is its amplitude. In a linear stability analysis, we use Eq. (8) in Eq. (6) and obtain a condition such that the energy expression up to quadratic order in α_k is negative. The average electrostatic $\langle \Pi_{ES} \rangle$ energy per unit area of the film can now be evaluated as

$$\langle \Pi_{ES} \rangle = -\frac{1}{2}\frac{(\varepsilon_p - 1)^2 \varepsilon_0 \varepsilon_p \phi^2}{(\varepsilon_p d + h)^2}. \tag{9}$$

The average elastic energy per unit area for such a deformation field in an incompressible film has been evaluated in an earlier work [26]:

$$\langle \Pi_{EL} \rangle = \frac{1}{2}\frac{\mu}{h} S(hk)\alpha_k^2, \tag{10}$$

where S(ζ) is the "universal function"

$$S(\zeta) = \frac{2\zeta(1 + \cosh(2\zeta) + 2\zeta^2)}{\sinh(2\zeta) - 2\zeta}. \tag{11}$$

The term $\mu S(hk)$ can be interpreted as a "wavelength (wavenumber) dependent effective elastic stiffness." The mean total energy per unit film area of the perturbation Eq. (8) is

$$\langle \Pi \rangle = \langle \Pi_{ES} \rangle + \langle \Pi_{ES} \rangle = \frac{1}{2}\left(\frac{\mu}{h} S(hk) - \frac{(\varepsilon_p - 1)^2 \varepsilon_0 \varepsilon_p \phi^2}{(\varepsilon_p d + h)^2}\right)\alpha_k^2. \tag{12}$$

If the term in the brackets becomes nonpositive, the perturbation Eq. (9) becomes unstable. The critical value of ϕ that induces instability is the smallest value of ϕ at which some mode (described by a wavenumber k) becomes unstable.

From the definition of S, it is evident that a perturbation wavelength is very small compared with the thickness $hk >> 1$ ($S(\zeta) \to \infty$, for $\zeta \to \infty$), and one with wavelength much larger than the film thickness $hk << 1$ ($S(\zeta) \to \infty$, for $\zeta \to 0$); both cost large energy penalties. The *lowest effective elastic stiffness* occurs at an intermediate value of the wavelength corresponding to $hk_c = 2.12$ for which $S(hk_c) = 6.22$. Thus, when the voltage ϕ exceeds a value ϕ_c, the perturbation with wavenumber equal to k_c or equivalently wavelength $\lambda_c \approx 3h$ becomes unstable, where ϕ_c is given by

$$\varphi_c^2 = \frac{6.22\mu}{h} \frac{(\varepsilon_p d + h)^3}{(\varepsilon_p - 1)^2 \varepsilon_p \varepsilon_0}. \tag{13}$$

Several important points may be noted.

1. The instability induced by the electric potential occurs at the same wavelength ($\lambda \sim 3h$) as that induced by the van der Waals forces. Thus, morphological changes induced by the electric field have similar spacing to that of the other adhesive interactions, including the van der Waals interaction. This observation is also in line with the linear stability analysis [21,24–33], which predicts the length scale of the elastic contact instability to be independent of the decay behavior of the adhesive force.
2. Because of the crack-like geometry in our experimental setup, it is evident that $\varepsilon_p d + h \approx h$ (because $d \sim 10$–$50\,\text{nm}$, $h \sim 10\,\mu\text{m}$, $\varepsilon_p \sim 3$), and thus

$$\phi_c = \left(\sqrt{\frac{6.22}{(\varepsilon_p - 1)^2 \varepsilon_0 \varepsilon_p}}\right) h\sqrt{\mu}. \tag{14}$$

We deduce, therefore, that the critical voltage necessary to induce morphological changes increases linearly with the thickness h of the film and has a weaker dependence on the shear modulus of the film as $\sqrt{\mu}$. Indeed, experiments shown in Figure 6 confirm the linear dependence of $\phi_c/\sqrt{\mu}$ as a function of film thickness, h. Interestingly, the case of pillar formation has a different slope, $(\mathrm{d}(\phi_c/\sqrt{\mu})/dh)$ compared with cases corresponding to the edge straightening and finger elongation. This difference is due to the geometry of the initial fingers. Even though their functional dependence on the film parameters such as film thickness and shear modulus is not modified, the energy magnitude changes. Our simplified analysis does indeed capture the linear behavior of $\phi_c/\sqrt{\mu}$ with h but does not account for the initial geometry of the finger pattern, and hence, the difference of the slopes in the two cases is not predicted.

3. For a film of thickness $h \sim 10\,\mu\mathrm{m}$, and gap distance $\mathrm{d} \sim 100\,\mathrm{nm}$, we estimate the critical voltage to be $\sim 2500\,\mathrm{V}$. This estimate is indeed within an order of magnitude of the experimental value of 200–500 V. As noted previously, the analysis has many approximations such as the neglect of the evolving electrostatic potential with deformation. Further, we have assumed that the contactor is rigid, whereas the contactor in our experiments is flexible and, consequently, our estimate of the critical voltage is expected to be larger

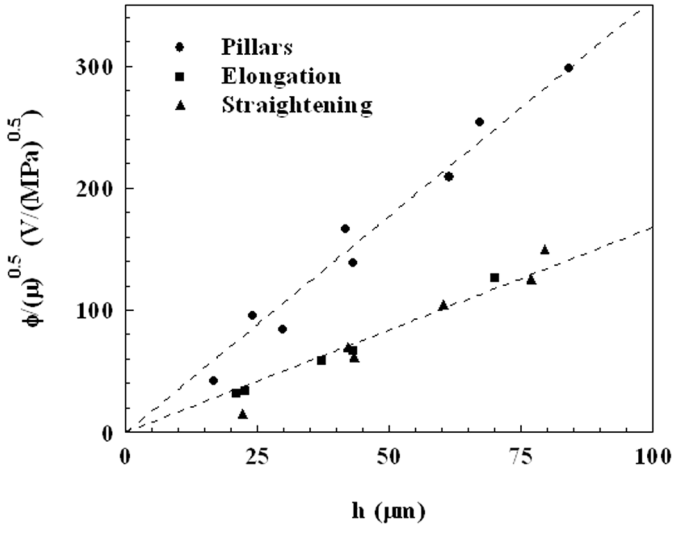

FIGURE 6 Plot of experimentally obtained $\phi_c/\sqrt{\mu}$ as a function of h from measurements of films of different h and μ values.

than what is seen in experiments. Therefore, we neither expect nor obtain quantitative agreement. However, as noted in the previous point, the predicted scaling of the critical voltage with the film thickness and shear modulus is expected to be more precise, as is indeed shown to be the case here.

We now turn to the explanation of the evolution of the morphology subsequent to the attainment of the critical voltage. As noted in the previous section, the morphological modifications effected by the electric field depends on the film stiffness parameter μ/h. For small values of μ/h, pillars are formed; intermediate μ/h gives finger elongation, and finally large μ/h produces edge straightening. To discuss these various morphologies, we now introduce an additional energy parameter, which was ignored thus far. The neglect of the bending energy of the flexible contactor in the calculation of the critical voltage (which assumed the contactor to be rigid) is a major reason for the overestimate of the critical voltage as already noted. While the electrostatic energy promotes the increase of the contact area between the film and the contactor, the resulting morphology depends on two forces, both of which act to oppose morphological changes—the elastic restoring forces in the film and the bending energy of the contactor. Although a quantitative estimate of the effect of the flexible contactor appears to be quite complex, we present qualitative arguments on its role, supported by appropriate simulations.

The final morphological structure depends on which of the two opposing forces are stronger. If the elastic stiffness parameter of the film and, consequently, the elastic energy penalty in the film are smaller than the energy penalty of the contactor bending, then the increase of contact area should occur by the deformation of the film surface, keeping the curved contactor in essentially the same configuration as before the application of the electric field. In our experiments, we do indeed see this scenario in the case of the pillar-formation regime for relatively small values of film stiffness. In this case, the initial areas of contact complete with the fingers are preserved, while pillars emerge ahead of the fingers. It is therefore evident that the contactor undergoes very little additional deformation in this case by the application of electric field. As seen from the morphological phase diagram, we note that the regime of small μ/h indeed produces pillar-like morphology when subjected to an external electric field.

On the other hand, in very stiff films (with large μ/h ratios), the contact area can be increased by deforming the contactor, rather than the film, so as to effectively move the contact line toward the spacer; *i.e.*, the average y-coordinate of the contact line increases (Figure 1).

Again, the regions of large μ/h do correspond to the edge straightening. For the intermediate values of the stiffness parameter μ/h, which is larger than the pillar-formation regime but smaller than the edge-straightening regime, the contactor bending energy penalty is comparable with the elastic energy penalty of the film. Thus, the contactor bends together with elongation of finger patterns, giving rise to labyrinth patterns, to gain the electrostatic energy.

We have been able to corroborate our qualitative arguments, albeit indirectly, by computer simulations of a rigid contactor. The key physical argument that allows us to relate the results of the rigid contactor simulations to the experiments is that the net result of contactor bending manifests as the change in the contactor curvature and the profile of the gap thickness and the average gap distance, d. It is evident that the average gap thickness (before the application of the electric field) depends inversely on the stiffness of the contactor. A less stiff contactor bends more during the adhesive contact, resulting in a steeper profile of the gap (higher curvature) and a higher average gap distance. When the bending stiffness of the contactor is large compared with the elastic stiffness of the film, the curvature that it acquires is small (so that the bending energy is reduced). On the other hand, in stiffer films, the curvature attained by the contactor will be larger. Thus, simulations with rigid curved contactors of different curvatures are expected to show different morphologies. For example, finger-type patterns are expected in the case where the contactor curvature is larger, and pillar-type patterns in the cases where the contactor curvature is smaller.

The simulations were performed for different curvature contactors by a direct minimization of the total energy given by Eq. (6). For a given ϕ, the energy-minimizing deformation field $u(x,y)$ was obtained. This was achieved by expanding the deformation field in a Fourier series and by finding the Fourier coefficients that minimize the energy using a conjugate gradient technique. Details of the numerical procedure are similar to the one-spatial-dimension simulations with a flat contactor given in Ref. [30]. The main difference is in the introduction of two spatial dimensions and a curved contactor.

Figures 7a and 7b show two types of morphologies obtained by simulations depending on the contactor curvature. The minimum energy pattern selected for larger contactor curvatures is indeed very similar to the elongated fingers seen in the experiments (Figure 2b). On the other hand, the patterns obtained for smaller contactor curvature is an array of circular pillars in a near hexagonal arrangement (Figure 2a). The spacing of the fingers and pillars in simulations are also always found to be three to four times the thickness of the film,

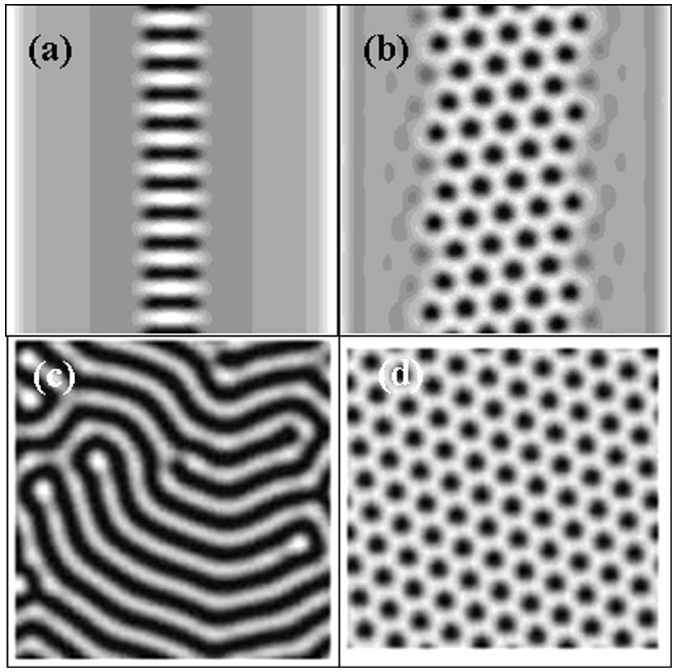

FIGURE 7 Simulations based on Eq. (7) showing the surface morphologies of a film at the onset of instability (thickness = 4 μm, $\phi = 500$ V, shear modulus = 0.1 MPa). These fully 2D simulations are performed on periodic square boxes 32 times the film thickness. The dark regions correspond to the film in contact with the top contactor. (a) Contactor curvature 9 units (compare with Figure 2b), showing finger-like patterns. (b) Contactor curvature 5 units, showing circular pillars in a nearly hexagonal arrangement (compare with Figure 2a). (c) Gap thickness d = 112 nm, showing finger-like morphology (compare with Figure 2b). (d) Gap thickness d = 133 nm, showing circular pillars in a nearly hexagonal arrangement (compare with Figure 2a).

which is again in agreement both with the linear stability analysis of a rigid, flat contactor, $\lambda \sim 3h$ and the experiments reported here. Thus, the simulations adequately mimic the basic physics of the influence of contactor stiffness by a change in the contactor curvature and its gap profile. The results of the simulations are also in agreement with the physical reasoning presented earlier, namely, that one expects the 2-D pillar regime for contactor stiffness to be large compared with the elastic stiffness of the film because of a smaller curvature of the contactor. In contrast, lower contactor stiffness mirrored in its higher curvature promotes finger-like patterns.

An even simpler model than that of the rigid curved contactor considered previously helps understanding of the pattern selection as the mean gap distance is increased. Figures 7c and 7d show two distinct types of morphologies depending on the gap thickness d as the distance between the contactor and the film increases. For a smaller gap thickness, the pattern that emerges is very similar to the elongated fingers seen in the experiments (Figure 2b), whereas for larger gap thickness, the pattern obtained is a set of circular pillars in a near hexagonal arrangement (Figure 2a). The spacing of the fingers and pillars in this simplified model is again about three times the thickness of the film. Basically, these simulations support the fact that contactor stiffness is large compared with the elastic stiffness of the film results in 2-D pillar patterns because of a larger mean gap distance, but the finger-like patterns are due to a smaller gap thickness. The minimun energy configuration in the energy landscape when the electirc field is applied corresponds to a set of parallel stripes. However, as has been shown in earlier work, the energy function is replete with many deep local minima. The process of minimization results in a configuration corresponding to local minima, which may represent the labyrinth pattern as shown in Figure 7c. A more detailed theoretical treatment of the couple contactor–film problem, including the bending stiffness of the contactor in a quantitative manner, is a fruitful direction for the future investigations.

We now turn to the discussion of the irreversibility of the patterns observed in some cases. This irreversibility refers to the lack of recovery of the original finger patterns upon switching off the applied voltage, as discussed in the previous section. We note that this phenomenon is due to the short-range van der Waals and other contact adhesive forces. The inclusion of short-range adhesive forces, after the formation of contact zones, generates metastable local minima in the energy landscape, which pins an already formed structure. Thus, after the formation of intimate contact zones, the structures already formed by the electric field can persist whenever the adhesive interactions are sufficient to maintain adhesion. Metastablity of adhesive zones, notwithstanding their higher energy, is also known to be responsible for the observed persistence of patterns in peeling and debonding experiments. The patterns once formed at elastic contact continue to adhere and elongate over much larger gap distances during the withdrawal or pulloff of the contactor [32]. The morphological patterns are thus trapped in a metastable local minimum of the energy, even though the global minimum of the energy after switching off the electric field is a flat film.

The driving force for the recovery and relaxation of the patterns after removal of the electric field or the contactor is the stored elastic

energy of the film. In the case of films with a small stiffness parameter that show pillar formation, these elastic forces are weak and are unable to move over the energy barrier that produces metastability. When the film stiffness parameter is large (resulting in edge-straightening effects upon the application of the electric field), the elastic forces are strong enough to drive the system back to its original configuration of finger patterns. In the intermediate case, the elastic forces provide for a partial recovery, but the system may get trapped in a metastable local energy minimum configuration intermediate to the original configuration and the one induced by the electric field.

5. CONCLUSIONS

We have reported detailed experiments, theory, and simulations on the morphological modulation of the elastic contact patterns by an applied electric field in a soft elastic film. It is found that three distinct types of electric-field-induced pattern morphologies are possible depending on the stiffness of the film. These include edge straightening (which reduces the dimensionality of the patterns), finger elongation (which maintains the dimensionality of the pattern), and pillar formation (which converts a 1D pattern into a 2D pattern). Our theoretical analysis based on elastic forces competing with the electrostatic force is able to predict the scaling of the critical voltage and the wavelength of the emergent pattern. Further, we provide qualitative arguments supported by energy minimization simulations to understand these morphological modifications brought about by a flexible electrode contactor.

Generally, the role of electric fields used to induce and modify the pattern morphology in liquid films has been extensively investigated [12–14,40]. The application of strong electric fields laterally between two capacitor plates produces forces that overcome the surface tension in thin liquid films, thereby inducing a characteristic pattern. The long-wave patterns in liquid films depend strongly on the field strength and its decay characteristics [12–14,40]. In contrast, the wavelength of the patterns in soft solid films does not depend on the strength of the electric field but depends only on the film thickness. The precise morphology, however, depends on the elastic stiffness of the films.

These novel effects introduced by an electric field on soft films suggest many technological applications and further scientific investigations. The ability to generate patterns that do not require patterned electrodes or a patterned medium can be an inexpensive route for large-area surface modification. Potential applications include

single-step, self-organized, meso-patterning of soft solid polymer films by the use of a prepatterned electrode contactor, electric-field-controlled "smart" adhesives, micropumps, and microfluidic applications.

ACKNOWLEDGMENTS

V. B. S. and A. S. acknowledge Department of Science and Technology, India, Nanoscience and Technology Program. K. S. N. and N. A. acknowledge H. M. Dixit for useful discussions.

REFERENCES

[1] Gent, A. N. and Petrich, R. P., *Proc. R. Soc. London. Ser.* A **310**, 433–448 (1969).
[2] Crosby, A. J., Shull, K. R., Lakrout, H., and Creton, C., *J. Appl. Phys.* **88**, 2956–2966 (2000).
[3] Lin, Y. Y., Hui, C.-Y., and Conway, H. D., *J. Polym. Sci., Part B: Polym. Phys.* **38**, 2769–2784 (2000).
[4] Chikina, I. and Gay, C., *Phys. Rev. Lett.* **85**, 4546–4549 (2000).
[5] Creton, C., Hooker, J., and Shull, K. R., *Langmuir* **17**, 4948–4954 (2001).
[6] Brown, K., Hooker, J. C., and Creton, C., *Macromol. Mater. Eng.* **287**, 163–179 (2002).
[7] McCabe, J. F., Carrick, T. E., and Kamohara, H., *Biomaterials* **23**, 1347–1352 (2002).
[8] Herminghaus, S., Jacobs, K., Mecke, K., Bischof, J., Fery, A., Ibn-Elhaj, M., and Schlagowski, S., *Science* **282**, 916–919 (1998).
[9] Sharma, A. and Khanna, R., *Phys. Rev. Lett.* **81**, 3463–3466 (1998).
[10] Reiter, G., Khanna, R., and Sharma, A., *Phys. Rev. Lett.* **85**, 1432–1435 (2000).
[11] Kargupta, K. and Sharma, A., *Phys. Rev. Lett.* **86**, 4536–4539 (2001).
[12] Schaffer, E., Thurn-Albrechet, T., Russell, T. P., and Steiner, U., *Nature* **403**, 874–877 (2000).
[13] Schaffer, E., Thurn-Albrechet, T., Russell, T. P., and Steiner, U., *Europhys. Lett.* **53**, 518–524 (2001).
[14] Morariu, M. D., Voicu, N. E., Schäffer, E., Lin, Z., Russell, T. P., and Steiner, U., *Nat. Mater.* **2**, 48–52 (2003).
[15] Asaro, R. J. and Tiller, W. A., *Metall. Trans.* **3**, 1789–1796 (1972).
[16] Srolovitz, D. J., *Acta Metall.* **37**, 621–625 (1989).
[17] Spencer, B. J., Voorhees, P. W., and Davis, S. H., *J. Appl. Phys.* **73**, 4955–4970 (1993).
[18] Craster, R. V. and Matar, O. V., *Phys. Fluids* **17**, 032104 (2005).
[19] Grinfield, M. A., *Sov. Phys. Dokl.* **31**, 831–834 (1986).
[20] Ramirez, J. C., *Int. J. Solids Struct.* **25**, 579–589 (1989).
[21] Ghatak, A., Chaudhury, M. K., Shenoy, V. B., and Sharma, A., *Phys. Rev. Lett.* **85**, 4329–4332 (2000).
[22] Shull, K. R., Flanigan, C. M., and Crosby, A. J., *Phys. Rev. Lett.* **84**, 3057–3060 (2000).
[23] Monch, E. and Herminghaus, S., *Europhys. Lett.* **53**, 525–531 (2001).
[24] Ghatak, A. and Chaudhury, M. K., *Langmuir* **19**, 2621–2631 (2003).
[25] Shenoy, V. B. and Sharma, A., *Phys. Rev. Lett.* **86**, 119–122 (2001).
[26] Shenoy, V. B. and Sharma, A., *J. Appl. Phy.* **94**, 6376–6385 (2003).

[27] Shenoy, V. B. and Sharma, A., *Langmuir* **18**, 2216–2222 (2002).
[28] Shenoy, V. B. and Sharma, A., *J. Mech. Phy. Solids* **50**, 1155–1173 (2002).
[29] Sarkar, J., Shenoy, V. B., and Sharma, A., *Phys. Rev. E* **67**, 031607 (2003).
[30] Sarkar, J., Sharma, A., and Shenoy, V. B., *J. Adhesion* **81**, 271–295 (2005).
[31] Sarkar, J., Sharma, A., and Shenoy, V. B., *Langmuir* **21**, 1457–1469 (2005).
[32] Sarkar, J., Shenoy, V. B., and Sharma, A., *Phys. Rev. Lett.* **93**, 018302 (2004).
[33] Ru, C., *J. Appl. Phys.* **90**, 6098–6104 (2001).
[34] Arun, N., Sharma, A., Shenoy, V. B., and Narayan, K. S., *Adv. Mater.* **18**, 660–663 (2006).
[35] Sia, S. K. and Whitesides, G. M., *Electrophoresis* **24**, 3563–3576 (2003).
[36] Xia, Y. and Whitesides, G. M., *Ann. Rev. Mater. Sci.* **28**, 153–184 (1998).
[37] Geissler, M. and Xia, Y., *Adv. Mater.* **16**, 1249–1269 (2004).
[38] Paul, D. T. H. and Shah, D. O., *Langmuir* **13**, 5995–5998 (1997).
[39] Griffiths, D. J., *Introduction to Electrodynamics*, 3rd ed. (Prentice-Hall, Englewood Cliffs, NJ, 1999), Chap. 2, pp. 103–106.
[40] Verma, R., Sharma, A., Kargupta, K., and Bhaumik, J., *Langmuir* **21**, 3710–3721 (2005).